



Fully doctor-bladed efficient organic solar cells processed under ambient condition

Xiaotong Guo^a, Hengyue Li^a, Yunfei Han^b, Yu Yang^a, Qun Luo^{b,**}, Chang-Qi Ma^b, Junliang Yang^{a,*}

^a Hunan Key Laboratory for Super-microstructure and Ultrafast Process, School of Physics and Electronics, Central South University, Changsha, 410083, China

^b Printable Electronics Research Center, Suzhou Institute of Nano-Tech and Nano-Bionics, Chinese Academy of Sciences, Suzhou, 215123, China

ARTICLE INFO

Keywords:

Organic solar cells
Doctor blading
Fully printing
Ambient condition

ABSTRACT

The low-cost and high-throughput printing techniques are potentially used to process large-area organic solar cells (OSCs). However, high-performance OSCs fabricated via fully printing process have lots of challenges. Herein, OSCs are fabricated via fully doctor blading using subsequently printed electron transport layer (ETL) zinc oxide (ZnO), printed bulk heterojunction (BHJ) active layer composed of poly[(2,6-(4,8-bis(5-(2-ethylhexyl)thiophen-2-yl)-benzo[1,2-b:4,5-b']dithiophene))-alt-(5,5-(1',3'-di-2-thienyl-5',7'-bis(2-ethylhexyl)benzo[1',2'-c:4'5'-c']dithiophene-4,8-dione))] (PBDB-T) and 3,9-bis(2-methylene-(3-(1,1-dicyano-methylene)-5-methylindane)-5,5,11,11-tetrakis(4-hexylphenyl)-dithieno[2,3-d:2',3'-d']-s-indaceno[1,2-b:5,6-b']-dithiophene (IT-M), and printed hole transport layer (HTL) molybdenum oxide (MoO₃). Through the optimization of inks and printing parameters, as well as humidity control, OSCs fabricated via printed ETL ZnO in ambient condition and spin-coated BHJ PBDB-T:IT-M in glovebox produce a power conversion efficiency (PCE) of 10.73%, which is similar to fully spin-coated device. While OSCs fabricated via printed ETL ZnO and BHJ PBDB-T:IT-M in ambient condition can produce a PCE of 10.15%. Furthermore, the PCE up to 9.34% can be achieved for fully printed OSCs with doctor-bladed ETL ZnO, BHJ PBDB-T:IT-M and HTL MoO₃ in ambient condition. These results suggest that high-performance OSCs can be fabricated using printing techniques in ambient condition instead of spin-coating and inert atmosphere, exhibiting great potential to accelerate the commercialization of OSCs.

1. Introduction

Organic solar cells (OSCs) have been attracting much attention and show potential applications because of many advantages such as light weight, semitransparency, solution-process ability, excellent compatibility with flexible substrate and roll-to-roll processing [1–5]. Due to the difficulties in synthesis and purification of fullerene acceptor materials, weak absorption in visible and near infrared region and poor coordination of energy levels, non-fullerene acceptor materials including small molecule and polymer are being developed rapidly [6–10]. Currently, the power conversion efficiencies (PCEs) over 17% have been achieved for single-junction OSCs based on non-fullerene acceptors [11], which is much higher than the conventional fullerene based OSCs, and the PCE of non-fullerene OSC modules also exceeds 10% [12]. However, these highly efficient OSCs are usually fabricated via spin-coating deposition in inert environment. Meanwhile, the electron transport layer (ETL) or

hole transport layer (HTL) is deposited via vacuum thermal evaporation. These fabrication processes do not match with large-scale fabrication with high throughput, which is not helpful to accelerate the industrialization of OSCs.

The scalable printing techniques, instead of conventional spin-coating or vacuum deposition, are attracting much more interesting to fabricate efficient OSCs, especially the fully-printed OSC devices. Several scalable printing techniques have been developed, including spray-coating, slot-die coating, inkjet printing, blade-coating, screen printing, roll-to-roll printing, and so on, which are widely used in fabricating light-emitting devices [13–15], field effect transistors [16, 17], supercapacitor [18,19] and solar cells [20–24]. However, most of reports about printed OSCs are focused on printing single active layer, while not fully printed OSCs including active layer, ETL and HTL [25–28]. The fully printed process, especially under ambient condition, is crucial for the large-scale industrialization of OSCs.

* Corresponding author.

** Corresponding author.

E-mail addresses: qluo2011@sinano.ac.cn (Q. Luo), junliang.yang@csu.edu.cn (J. Yang).

<https://doi.org/10.1016/j.orgel.2020.105725>

Received 19 December 2019; Received in revised form 18 February 2020; Accepted 15 March 2020

Available online 23 March 2020

1566-1199/© 2020 Elsevier B.V. All rights reserved.

In order to achieve fully printed OSCs under ambient condition, one of big challenge issues is to deposit ETL or HTL on the active layer via printing process instead of conventional spin-coating or vacuum deposition because of the hydrophobicity of the active layer. For example, in inverted OSCs with a structure of ITO/ETL/active layer/HTL/Ag, metal oxides such as titanium oxide (TiO_2) and zinc oxide (ZnO) have been used as the ETL for improving the stability [29–31], the conventional hydrophilic PEDOT:PSS as the HTL is normally difficult to deposit on hydrophobic active layer directly via spin-coating or printing process. Thus, it is necessary to use surfactants and additives to adjust the surface tension of PEDOT:PSS solution and enhance its wettability on the surface of active layer, accordingly improve the device performance [32]. But the addition of the surfactants or additives would bring an additional problem of removing these additives later. Hence, metal oxides are accepted as the alternative of PEDOT:PSS in inverted OSCs, such as molybdenum oxide (MoO_3), vanadium oxide (V_2O_5), tungsten oxide (WO_3) [33–35]. In most cases, these metal oxide layers are deposited by thermal evaporation and the thickness is limited of 5–10 nm. Thus, the development of printable metal oxides solution in fully printed inverted OSCs becomes important. On the other hand, it is very meaningful to understand the influence of ambient environment on the fabrication of OSCs. The high-performance OSCs are normally prepared in nitrogen-protected environment, avoiding the influence of ambient condition including humidity and oxygen. Meanwhile, the PCEs of doctor-bladed OSCs are much lower than those of spin-coated OSCs [36, 37]. Thus, it is important to explore the influence of humidity on the performance of printed OSCs, and the precise optimization of ambient condition including humidity and temperature is a key step to the development of printed OSCs.

Herein, highly efficient OSCs with a configuration of ITO/ ZnO /active layer/ MoO_3 /Ag (Fig. 1a) were fabricated via fully printing processes using doctor blading (Fig. 1b) in ambient condition with control humidity, in which the active layer is bulk heterojunction (BHJ) composed of poly[(2,6-(4,8-bis(5-(2-ethylhexyl) thiophen-2-yl)-benzo[1,2-b:4,5-b']dithiophene))-alt-(5,5-(1',3'-di-2-thienyl-5',7'-bis(2-ethylhexyl)benzo[1',2'-c:4'5'-c']dithiophene-4,8-dione))] (PBDB-T, Fig. 1c) and 3,9-bis(2-methylene-(3-(1,1-dicyano-methylene)-5-methylindanone)-5,5,11,11-tetrakis(4-hexylphenyl)-dithieno[2,3-d:2',3'-

d']-s-indaceno[1,2-b:5,6-b']-dithiophene (IT-M, Fig. 1c). Meanwhile, a low-temperature and solution-processed MoO_3 as the HTL was well deposited on BHJ PBDB-T:IT-M via doctor blading, forming a good wettable and uniform thin film. With control humidity under ambient condition, high-performance fully doctor-bladed OSCs with a PCE up to 9.34% could be achieved. More importantly, the influence of humidity on the morphology evolution and device performance of doctor-bladed PBDB-T:IT-M under ambient condition was explored. The research paves a good way to achieve fully printed OSCs via doctor blading, which is helpful to the potential industrialization of OSCs.

2. Results and discussions

BHJ OSCs with a device architecture of ITO/ ZnO /PBDB-T:IT-M/ MoO_3 /Ag were fabricated, as illustrated in Fig. 1a. In order to achieve fully printed OSCs, the ETL ZnO , the active layer PBDB-T:IT-M and the HTL MoO_3 can be subsequently deposited by doctor blading (Fig. 1b) under ambient condition with control humidity, except for the Ag electrode. The molecular structures of polymer PBDB-T and non-fullerene small molecule acceptor IT-M are showed in Fig. 1c.

The ETL ZnO ink formulation was prepared according to our previous work [38]. Before doctor blading ZnO thin film, the ITO substrate temperature was increased to 60 °C for improving solvent volatilization during doctor blading and forming a homogenous thin film. With optimizing the blading speed, a uniform and transparent ZnO layer could be formed. Under the certain concentration of ink solution, the thickness of ZnO layer can be controlled by the blading speed. As showed in Fig. S1 and Table S1, the thickness of doctor-bladed ZnO can be controlled from 10 nm to 40 nm, and the PCEs of OSCs with spin-coated PBDB-T:IT-M and vacuum-evaporated MoO_3 could remain to be over 10%, exhibiting less thickness dependence, and they are comparable to the control one with spin-coated ZnO layer. If the doctor-bladed ZnO is too thin to cover the ITO, there is a certain degree of defects, and the performance of OSCs would be influenced. Thus, the OSCs with doctor-bladed 10 nm ZnO exhibit the lowest PCE, which is just about 10%. On the other hand, the very thick ZnO layer would reduce the conductivity due to the intrinsic properties, leading to damping of device performance [39]. The optimized thickness of doctor-bladed ZnO was set to be about 30 nm, which

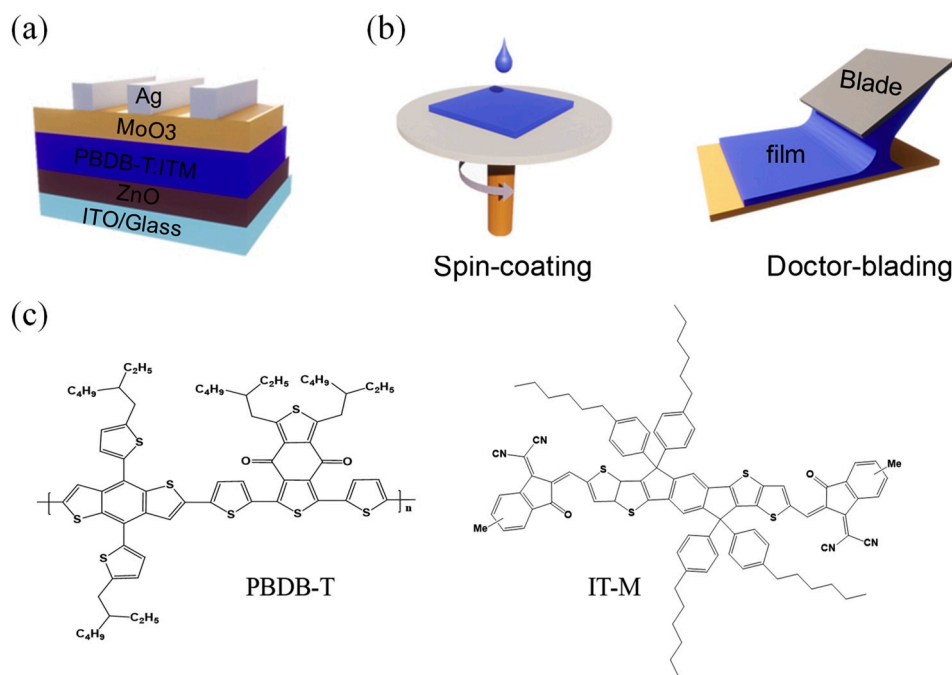


Fig. 1. (a) Schematic of BHJ OSCs with a structure of ITO/ ZnO /PBDB-T:IT-M/ MoO_3 /Ag. (b) Schematics of spin-coating and doctor blading. (c) Chemical structures of polymer PBDB-T and small molecule acceptor IT-M.

is used for fabricating OSCs subsequently.

AFM can be used to well observe the morphology and microstructure of functional thin films [40]. Fig. 2a and b show surface morphology of doctor-bladed and spin-coated ZnO thin films, respectively. Both thin films show a very similar surface topography and the root-mean-square (RMS) roughnesses are 2.00 nm and 2.37 nm, respectively. Meanwhile, their 3D morphologies are showed in Fig. 2c and d as well. These results suggest that the doctor-bladed ZnO thin film is as smooth as the one deposited via spin coating. Furthermore, the transmittance spectra exhibit nearly the same optical characteristics for both ZnO thin films, as shown in Fig. 2e. The transmittance is more than 80% in the wavelength range of 500 nm–800 nm, which allows OSCs to make good use of light without being affected by the ETL layer. Thus, high-quality ZnO thin film can be deposited by doctor-blading process.

The morphology and thickness of BHJ active layer can greatly influence the performance of OSCs [41,42]. For depositing the active layer under ambient condition via doctor blading, more attention should be paid to the influence of humidity on organic active thin film, which is one of the key factors affecting the thin film morphology and accordingly the performance of OSCs. Thus, the BHJ PBDB-T:IT-M thin films are deposited under three kinds of humidity conditions, *i.e.*, 0.1 ppm (glove box), ~35%, and ~75%. The J-V characteristics of OSC devices are showed in Fig. 3a and the corresponding photovoltaic parameters are summarized in Table 1. Under the humidity of 0.1 ppm, the PCE of device prepared with doctor-bladed ZnO thin film and spin-coated PBDB-T:IT-M is 10.73% with an open-circuit voltage (V_{oc}) of 0.92 V, a short-circuit current density (J_{sc}) of 16.30 mA cm⁻², and a fill factor (FF) of 0.716. The OSCs fabricated by doctor blading under the humidity of ~75% exhibit very poor photovoltaic performance parameters with a

V_{oc} of 0.88 V, a J_{sc} of 15.00 mA cm⁻², an FF of 0.641, resulting in a PCE of 8.45%. As the environment humidity was controlled to ~35%, the device shows an improved PCE of 10.15%, with a V_{oc} of 0.92 V, a J_{sc} of 16.50 mA cm⁻² and an FF of 0.672. The results suggest that the humidity in atmosphere can seriously influence the performance of OSCs. The external quantum efficiency (EQE) spectra of the resulted devices are illustrated in Fig. 3b for evaluating the photon-to-electron conversion efficiency. All the devices show similar EQE spectra over 300–800 nm wavelength and the EQE values increase with the decreasing humidity during the device fabrication, resulting in the improved J_{sc} . The integrated J_{sc} values calculated from EQE are 15.34 mA cm⁻², 15.53 mA cm⁻² and 14.10 mA cm⁻², respectively, which are very close to the values measured from J-V curves.

It is worth noting that the absorption is a bit different for the three kinds of BHJ PBDB-T:IT-M thin films from the ultraviolet–visible absorption spectra (UV–vis). In Fig. 3c, the light absorption of PBDB-T:IT-M thin film prepared with 0.1 ppm is a little weaker at the peak. It may be due to the thin-film thickness of spin-coated PBDB-T:IT-M is about 100 nm, while the doctor-bladed ones have a relatively high thickness of about 120 nm. It is well known that the thicker film can enhance the light absorption. But, as the active layer exceeds a certain thickness, it would increase the carrier diffusion length. Thus, more charge recombination will occur in the active layer, causing the decrease in V_{oc} and FF , eventually resulting in the degradation in device performance [43].

After the PBDB-T:IT-M thin film was doctor bladed onto ZnO, thermal annealing was performed at 150 °C for 30 min in glovebox. The film thickness of active layer is about 120 nm and the optimized thickness is shown in Fig. S2 and Table S2. It can be seen that the OSCs can achieve PCEs more than 9% as the active layer thickness is increased from 90 nm

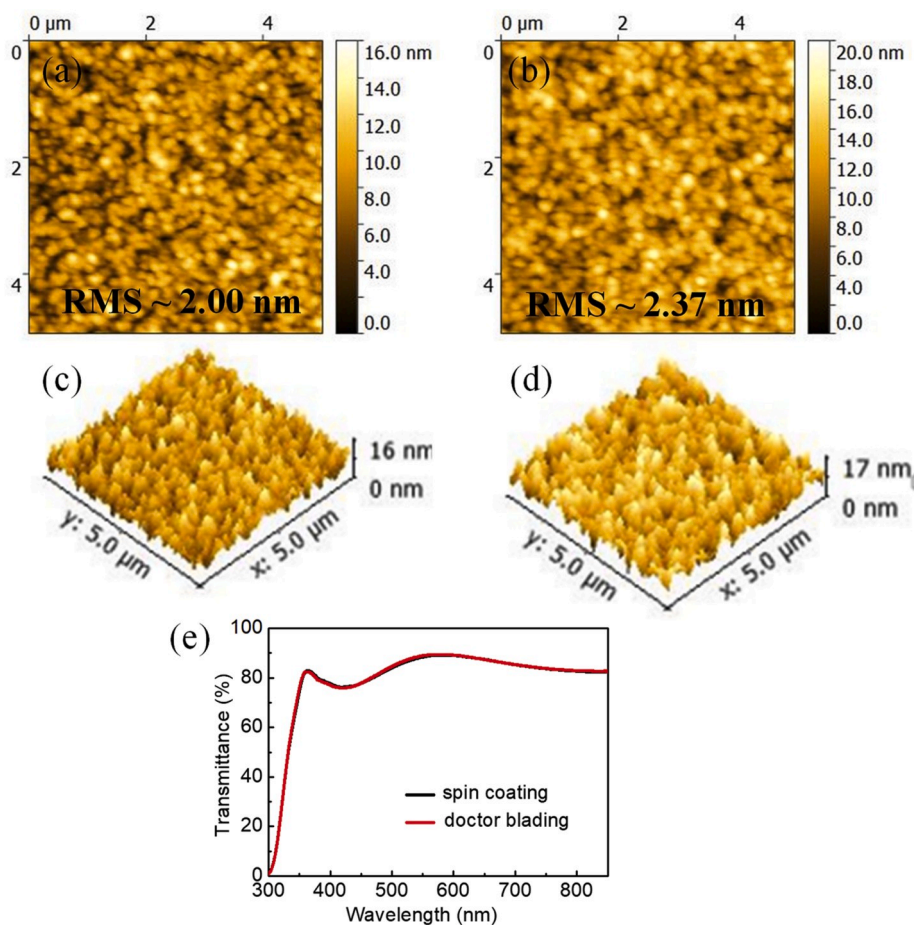


Fig. 2. AFM images of ZnO thin films deposited via spin-coating in glovebox (a, c) and doctor blading under ambient condition at a substrate temperature of 60 °C (b, d), respectively. (e) Transmittance spectra of spin-coated and doctor-bladed ZnO thin films.

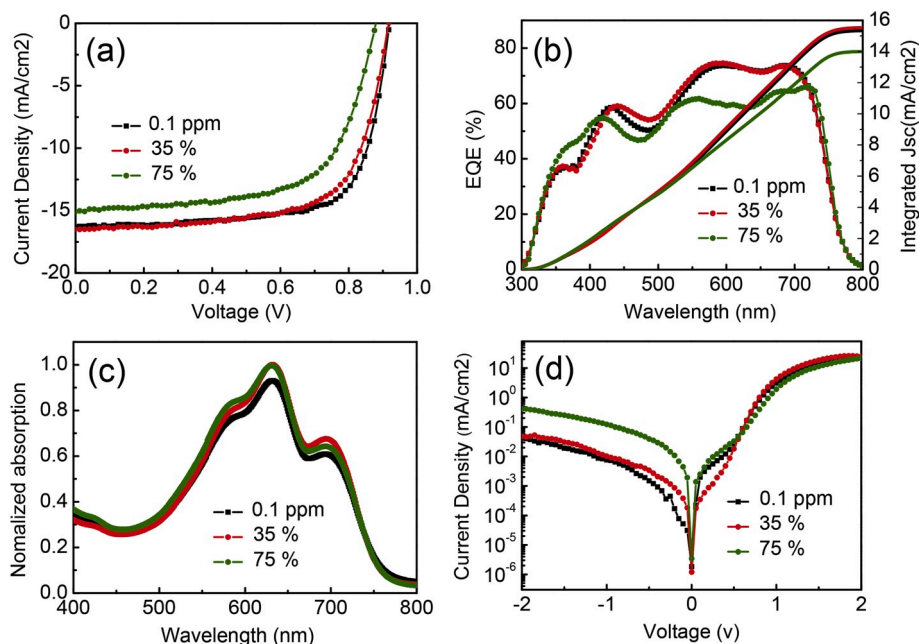


Fig. 3. (a) J-V curves, (b) EQE spectra, (c) UV-vis absorbance curves and (d) J-V curves in the dark for PBDB-T:IT-M OSCs fabricated via spin-coating in glovebox (humidity of 0.1 ppm) and doctor blading in ambient condition under the humidity of about 35% and 75%, respectively.

Table 1

Device performance parameters of OSCs for PBDB-T:IT-M thin films fabricated on doctor-bladed ZnO layer via spin-coating in glovebox (humidity of 0.1 ppm) and doctor blading in ambient condition under the humidity of about 35% and 75%, respectively. The average values are obtained from 10 devices, and integrated J_{cal} are derived from the EQE curves.

Deposition	V_{oc} (V)	J_{sc} (mAcm^{-2})	J_{cal} (mAcm^{-2})	FF (%)	PCE_{max} (%)	PCE_{ave} (%)
Spin-coating (0.1 ppm)	0.92	16.30	15.34	71.6	10.73	10.57 \pm 0.13
Doctor blading (~35%)	0.92	16.50	15.53	67.2	10.15	10.03 \pm 0.10
Doctor blading (~75%)	0.88	15.00	14.10	64.1	8.45	8.24 \pm 0.11

to 300 nm, indicating that the PBDB-T:IT-M system has a certain extent tolerance to the thickness. The J-V characteristics of OSCs measured in the dark are shown in Fig. 3d. The device fabricated under high humidity of ~75% shows the highest leakage current in the reverse direction, while the devices fabricated under the humidity of ~35% or in glovebox exhibit a lower leakage current. The results suggest that a better charge transport and extraction with the reduced hole and electron recombination for the OSCs fabricated under a low humidity. The leakage current decreases with decreasing the humidity, which plays an important role in raising the V_{oc} and FF in OSCs [44–46]. Thus, the overall photovoltaic performance can be enhanced for the OSCs fabricated under low humidity condition. All these results also indicate that it is no necessary to fabricate OSCs under the inert atmosphere, the high-performance OSCs can be fabricated in ambient condition with controllable humidity, which would greatly decrease the cost for accelerating the potential large-scale, industrial production of OSCs.

Furthermore, the surface morphology of PBDB-T:IT-M thin films deposited under the different conditions on the ZnO was studied by AFM and scanning electron microscopy (SEM), and the respective images are shown in Fig. 4 and Fig. S3. Fig. 4a–c are AFM images of PBDB-T:IT-M thin films and the inset are phase images. It is very obvious that the AFM morphology of PBDB-T:IT-M thin film prepared via doctor blading

under the humidity of ~35% is similar to that of the one prepared by spin coating in glovebox. The two PBDB-T:IT-M thin films exhibit similar phase-separation morphologies and granular aggregates of similar sizes, as seen from the inset phase images, which would be beneficial for efficient exciton dissociation [47]. With the increase of humidity to ~75%, the doctor-bladed PBDB-T:IT-M thin film is no longer flat and dense. The surface is very rough and the phase separation scale becomes significantly larger. The RMS values of three PBDB-T:IT-M thin films are 2.69 nm, 5.59 nm and 11.15 nm, respectively, with increasing the humidity. The AFM results indicate that the doctor blading under controllable humidity can produce a flat and dense thin film as effectively as spin coating, which is favorable to form a good contact between the cathode, HTL and the active layer. Fig. S3 shows the top-view SEM images of PBDB-T:IT-M on the ZnO fabricated via spin-coating in glovebox with 0.1 ppm humidity and doctor blading in ambient condition under the humidity of ~35% and ~75% humidity, respectively. The PBDB-T:IT-M thin films show flat surface and there are very few “island”, which would be well compatible with the ETL and HTL. As the humidity was enhanced ~75%, a few holes appear in doctor-bladed PBDB-T:IT-M thin film, as indicated with the circles. These defects probably lead to serious charge recombination, reducing the carrier transport and collection, which is consistent with AFM images and the low performance parameters J_{sc} , V_{oc} and FF. The AFM and SEM morphology images clearly suggest that the humidity in the atmosphere has a serious impact on the thin-film formation process. By controlling humidity, the defects can be largely suppressed, leading to the OSCs with good performance.

After the deposition of the active layer PBDB-T:IT-M thin film, the HTL was sequentially deposited via the optimized doctor-blading process as the same of the ETL ZnO. The MoO₃ instead of conventional PEDOT:PSS was used as the HTL because of the critical inherent difficulties involving the wettability of the hydrophilic PEDOT:PSS onto the hydrophobic photoactive layer. The formation of good MoO₃ thin film can be attributed to the excellent wetting property of the MoO₃ solution on the surface of PBDB-T:IT-M thin film. As shown in Fig. S4, the MoO₃ solution can immediately spread and the contact angle is about 22° on the active layer, implying the complete wetting of the MoO₃ solution on PBDB-T:IT-M. Fig. S5 shows the cross-sectional SEM image of the fully printed OSC device via doctor blading. Each layer of OSC device can be

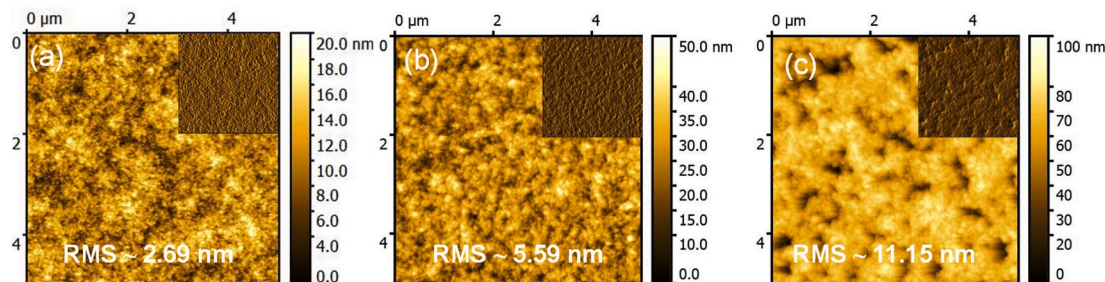


Fig. 4. AFM morphology images of PBDB-T:IT-M blend thin films fabricated via (a) spin-coating in glovebox with 0.1 ppm humidity and doctor blading in ambient condition under the humidity of (b) $\sim 35\%$ and (c) $\sim 75\%$ humidity, respectively. The inserts are their phase images.

clearly seen. The MoO_3 layer exhibits a continuous and uniform film that contacts with the active layer, which would not only lead to the high-performance OSCs, but also contribute to the excellent reproducibility of OSCs. Thus, the fully-printed OSCs show the PCE up to 9.34% with a V_{oc} of 0.89 V, a J_{sc} of 16.38 mA cm^{-2} , and an FF of 0.644. The J - V and EQE are shown in Fig. 5a and b. The integrated J_{sc} value calculated from EQE is 15.47 mA cm^{-2} , which can be consistent with the value measured from the J - V curve.

One may notice that the significant loss in the PCE mainly result from the sharp drop in FF . The FF is decreased from 0.716 to 0.644, about 10% decrease, when the number of doctor-bladed thin films in OSCs from 1 layer to 3 layer, as shown in Table S3. The electrochemical impedance spectroscopy (EIS) analysis was used to analyze the interface resistance of printed OSCs. The equivalent circuit model used for the EIS fitting is shown in Fig. 5c. The charge-transfer resistance (R_{ct}) is related to the diameter of the semicircles [26,48]. As shown in Fig. 5d, it can be seen that impedance spectroscopy of OSCs based on only doctor-bladed ZnO layer shows the smallest diameter, indicating the smallest R_{ct} resistance. The diameter of impedance spectroscopy increases along with the number of doctor-bladed layers. The large diameter in doctor-bladed OSCs indicates a poor interfacial contact, which is consistent with the decreased FF . This phenomenon is in good agreement with the measured results from J - V curve. From Table S3, the OSC devices with only doctor-bladed ZnO layer show a relatively low series resistance ($R_s \approx$

$42.2 \Omega \text{ cm}^2$) and high shunt resistance ($R_{sh} \approx 12541 \Omega \text{ cm}^2$). As using two doctor-bladed layers, *i.e.*, ZnO layer and PBDB-T:IT-M layer, to structure the OSCs, the R_s rises to $60.8 \Omega \text{ cm}^2$ and R_{sh} decreases to $9623 \Omega \text{ cm}^2$. The R_s and R_{sh} of fully printed OSC device, *i.e.*, doctor-bladed ZnO layer, PBDB-T:IT-M layer and MoO_3 layer, are $83.1 \Omega \text{ cm}^2$ and $8404 \Omega \text{ cm}^2$, respectively. With increasing the number of doctor-bladed layer from 1 to 3, the R_s increases dramatically while the R_{sh} decreases. It indicates that the interface contact resistance increases dramatically as increasing the number of doctor-bladed layer, leading to the obvious decrease in FF [49]. The results are consistent with the analysis on AFM and SEM morphology above.

3. Conclusion

In summary, doctor-blading process in ambient condition is demonstrated to assemble OSCs with a structure of ITO/ZnO/PBDB-T:IT-M/ MoO_3 /Ag, completely free from spin-coating techniques. The morphology of active layer PBDB-T:IT-M could be adjusted by the humidity in ambient condition. When the humidity is controlled at $\sim 35\%$, the resulted OSCs exhibit a high PCE up to 10.15%, which is comparable to that of OSCs fabricated by conventional spin-coating in glovebox. Furthermore, the HTL MoO_3 was also deposited via doctor blading, instead of conventional vacuum evaporation, on the PBDB-T:IT-M, leading to fully printed OSCs in ambient condition with a PCE of

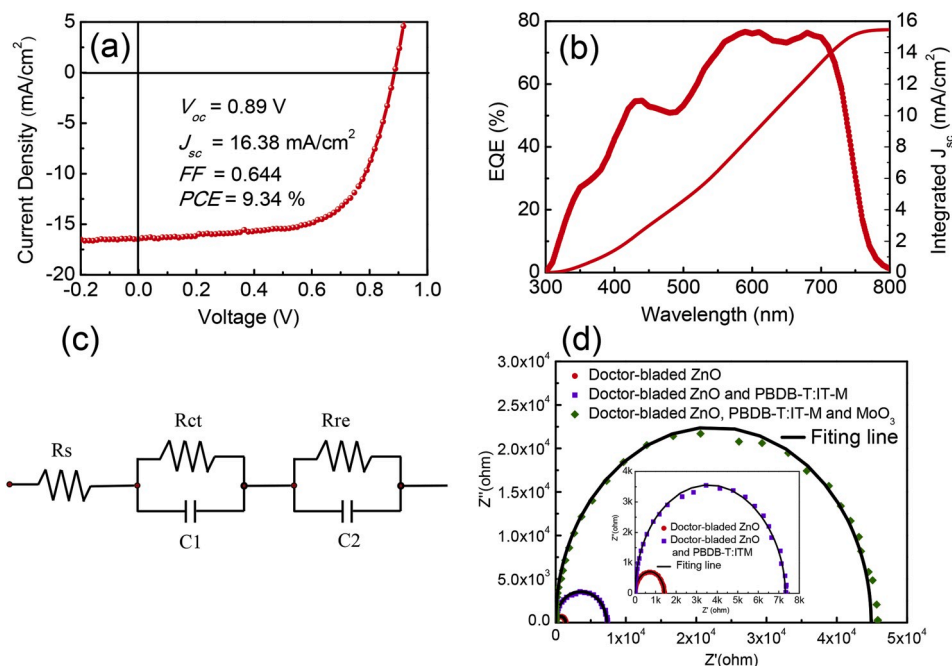


Fig. 5. (a) J - V curve and (b) EQE spectra of typical fully doctor-bladed OSC. (c) The equivalent-circuit model employed for the EIS fitting of OSCs. (d) Nyquist plots (symbols) and fitting curves (solid lines) of OSCs with doctor-bladed ZnO, doctor-bladed ZnO and PBDB-T:IT-M, and doctor-bladed ZnO, PBDB-T:IT-M, and MoO_3 .

9.34%, maintaining about 90% of original PCE for OSCs fabricated via spin coating under inert atmosphere condition. These results illustrate that it is feasible to prepare high-performance BHJ OSCs by large-scale, low-cost doctor blading in ambient condition, exhibiting the potentially practical application.

Declaration of competing interest

The authors declare that they have no known competing financial interests or personal relationships that could have appeared to influence the work reported in this paper.

Acknowledgements

This work is supported by the National Key Research and Development Program of China (2017YFA0206600) and the National Natural Science Foundation of China (51673214).

Experimental section

Materials: Polymer PBDB-T and non-fullerene small molecule acceptor IT-M were purchased from Solarmer Materials Inc. The number average molecular weight (M_n) and the mass average molecular weight (M_w) of polymer PBDB-T are 12.1 kDa and 21.9 kDa, respectively. ZnO and MoO₃ inks were synthesized according to our previous work [38, 50]. The other solvents including chlorobenzene (99.8%, Sigma-Aldrich) and 1, 8-Diiodooctane (95%, TCI) were used as received and without further treatment.

Device Fabrication: The patterned indium tin oxide (ITO, 15 Ω sq⁻¹) coated glass was used as the substrate, and was cleaned by ultrasound sequentially with acetone, detergent, deionized water, and isopropanol alcohol for 20 min, respectively. Then, the ITO glass was further treated by a UV-ozone cleaner for 25 min after drying with a nitrogen flow. For the ETL, 30 μ L precursor was dropped on the substrate and the blade coater was then moved to spread the ZnO ink and control the film thickness. The speed of blade coating was kept at 21 mm s⁻¹. After the thin film was formed, it was annealed at 170 °C for 10 min in ambient condition. For comparison, ZnO thin film of the control one was deposited by using the conventional spin-coating with the same precursor solution, others are as the same as the printed devices. The active layer was deposited by the mixture solution of PBDB-T: IT-M (10 mg: 10 mg in 1 mL chlorobenzene with 1% vol DIO and stirred over night) with a coating speed of 8 mm s⁻¹, followed by a heat-treatment at 150 °C for 30 min in glovebox. After the active layer was cooled down, the MoO₃ solution was doctor-bladed with the same speed of the ZnO layer and without further annealing. At last, a 100 nm thick Ag electrode was deposited via thermal evaporation with a mask at a pressure of 8×10^{-4} mbar, resulting in an active area of 0.09 cm². All the doctor-blading processes were performed on the hot stage at 60 °C under ambient condition with controlled humidity, which was controlled by a dehumidifier in a closed space.

Characterization: The doctor-blading process was performed with a commercial machine (ZN320, Maosen, Fujian). Ultraviolet-visible spectrophotometer (UV-vis, Puxi, T9, China) was employed to characterize the absorption and transmittance spectra of PBDB-T:IT-M and ZnO layer, respectively. Atomic force microscope (Agilent Technologies 5500 AFM/SPM System, USA) and scanning electron microscope (FEI Helios Nanolab 600i, SEM, USA) was employed to characterize surface morphology and RMS roughness of ZnO and PBDB-T:IT-M thin films. The film thickness was measured by a surface profilometer (DektakXT, BRUKER, USA). Current density-voltage (J-V) characteristics of OSCs were measured by digital source meter (Keithley, model 2400, USA). The measurement was carried out by a Xenon-lamp-based solar simulator (Newport 91160s, AM 1.5 G) with a light intensity of 100 mW/cm², which was calibrated by a standard silicon solar cell. Incident photon to current conversion efficiency (IPCE, Saifan, Beijing) spectra of OSC

devices were performed and analyzed by quantum efficiency measurement system. Dark J-V curves were measured by semiconductor characteristics system (Keithley, SCS-4200). Impedance spectra were measured by electrochemical workstation (CH Instruments, Shanghai Chenhua instrument Corporation, China). All characterizations of OSCs were carried out in ambient condition without encapsulation.

Appendix A. Supplementary data

Supplementary data to this article can be found online at <https://doi.org/10.1016/j.orgel.2020.105725>.

References

- [1] G. Li, R. Zhu, Y. Yang, Polymer solar cells, *Nat. Photon.* 6 (3) (2012) 153–161.
- [2] J. Yang, D. Vak, N. Clark, J. Subbiah, W.W.H. Wong, D.J. Jones, S.E. Watkins, G. Wilson, Organic photovoltaic modules fabricated by an industrial gravure printing proofer, *Sol. Energy Mater. Sol. Cells* 109 (2013) 47–55.
- [3] G. Yu, J. Gao, J.C. Hummelen, F. Wudl, A.J. Heeger, Polymer photovoltaic cells: enhanced efficiencies via a network of internal donor-acceptor heterojunctions, *Science* 270 (5243) (1995) 1789–1791.
- [4] J.Y. Kim, K. Lee, N.E. Coates, D. Moses, T.-Q. Nguyen, M. Dante, A.J. Heeger, Efficient tandem polymer solar cells fabricated by all-solution processing, *Science* 317 (5835) (2007) 222–225.
- [5] J. Xiong, B. Yang, J. Yuan, L. Fan, X. Hu, H. Xie, L. Lyu, R. Cui, Y. Zou, C. Zhou, D. Niu, Y. Gao, J. Yang, Efficient organic photovoltaics using solution-processed, annealing-free TiO₂ nanocrystalline particles as an interface modification layer, *Org. Electron.* 17 (2015) 253–261.
- [6] Y. Lin, J. Wang, Z.-G. Zhang, H. Bai, Y. Li, D. Zhu, X. Zhan, An electron acceptor challenging fullerenes for efficient polymer solar cells, *Adv. Mater.* 27 (7) (2015) 1170–1174.
- [7] H. Zhang, H. Yao, J. Hou, J. Zhu, J. Zhang, W. Li, R. Yu, B. Gao, S. Zhang, J. Hou, Over 14% efficiency in organic solar cells enabled by chlorinated nonfullerene small-molecule acceptors, *Adv. Mater.* 30 (28) (2018), e1800613.
- [8] J. Yuan, Y. Zhang, L. Zhou, C. Zhang, T.K. Lau, G. Zhang, X. Lu, H.L. Yip, S.K. So, S. Beaupré, M. Mainville, P.A. Johnson, M. Leclerc, H. Chen, H. Peng, Y. Li, Y. Zou, Fused benzothiadiazole: a building block for n-type organic acceptor to achieve high-performance organic solar cells, *Adv. Mater.* 31 (17) (2019), e1807577.
- [9] J. Yuan, Y. Zhang, L. Zhou, G. Zhang, H.L. Yip, T.K. Lau, X. Lu, C. Zhu, H. Peng, P. A. Johnson, M. Leclerc, Y. Cao, J. Ulanski, Y. Li, Y. Zou, Single-junction organic solar cell with over 15% efficiency using fused-ring acceptor with electron-deficient core, *Joule* 3 (4) (2019) 1140–1151.
- [10] Y. Lin, S. Dong, Z. Li, W. Zheng, J. Yang, A. Liu, W. Cai, F. Liu, Y. Jiang, T. P. Russell, F. Huang, E. Wang, L. Hou, Energy-effectively printed all-polymer solar cells exceeding 8.61% efficiency, *Nano Energy* 46 (2018) 428–435.
- [11] NREL. <https://www.nrel.gov/pv/assets/pdfs/best-research-cell-efficiencies.20190923.pdf>.
- [12] W. Zhao, Y. Zhang, S. Zhang, S. Li, C. He, J. Hou, Vacuum-assisted annealing method for high efficiency printable large-area polymer solar cell modules, *J. Mater. Chem. C* 7 (11) (2019) 3206–3211.
- [13] S. Tong, H. Wu, C. Zhang, S. Li, C. Wang, J. Shen, S. Xiao, J. He, J. Yang, J. Sun, Y. Gao, Large-area and high-performance CH₃NH₃PbI₃ perovskite photodetectors fabricated via doctor blading in ambient condition, *Org. Electron.* 49 (2017) 347–354.
- [14] C. Jiang, Z. Zhong, B. Liu, Z. He, J. Zou, L. Wang, J. Wang, J. Peng, Y. Cao, Coffee-ring-free quantum dot thin film using inkjet printing from a mixed-solvent system on modified ZnO transport layer for light-emitting devices, *ACS Appl. Mater. Interfaces* 8 (39) (2016) 26162–26168.
- [15] Q. Hu, H. Wu, J. Sun, D. Yan, Y. Gao, J. Yang, Large-area perovskite nanowire arrays fabricated by large-scale roll-to-roll micro-gravure printing and doctor blading, *Nanoscale* 8 (9) (2016) 5350–5357.
- [16] C. Cao, J.B. Andrews, A.D. Franklin, Completely printed, flexible, stable, and hysteresis-free carbon nanotube thin-film transistors via aerosol jet printing, *Adv. Energy Mater.* 3 (5) (2017), 1700057.
- [17] M. Yu, H. Wan, L. Cai, J. Miao, S. Zhang, C. Wang, Fully printed flexible dual-gate carbon nanotube thin-film transistors with tunable ambipolar characteristics for complementary logic circuits, *ACS Nano* 12 (11) (2018) 11572–11578.
- [18] H. Li, H. Guo, S. Tong, K. Huang, C. Zhang, X. Wang, D. Zhang, X. Chen, J. Yang, High-performance supercapacitor carbon electrode fabricated by large-scale roll-to-roll micro-gravure printing, *J. Phys. D: Appl. Phys.* 52 (11) (2019), 115501.
- [19] W.J. Hyun, E.B. Secor, C.-H. Kim, M.C. Hersam, L.F. Francis, C.D. Frisbie, Scalable, self-aligned printing of flexible graphene micro-supercapacitors, *Adv. Energy Mater.* 7 (17) (2017), 1700285.
- [20] Y. Lin, C. Cai, Y. Zhang, W. Zheng, J. Yang, E. Wang, L. Hou, Study of ITO-free roll-to-roll compatible polymer solar cells using the one-step doctor blading technique, *J. Mater. Chem. A* 5 (8) (2017) 4093–4102.
- [21] Y. Peng, Y. Cheng, C. Wang, C. Zhang, H. Xia, K. Huang, S. Tong, X. Hao, J. Yang, Fully doctor-bladed planar heterojunction perovskite solar cells under ambient condition, *Org. Electron.* 58 (2018) 153–158.
- [22] L. Zhang, B. Lin, B. Hu, X. Xu, W. Ma, Blade-cast nonfullerene organic solar cells in air with excellent morphology, efficiency, and stability, *Adv. Mater.* 30 (22) (2018), e1800343.

- [23] Y. Lin, Y. Jin, S. Dong, W. Zheng, J. Yang, A. Liu, F. Liu, Y. Jiang, T.P. Russell, F. Zhang, F. Huang, L. Hou, Printed nonfullerene organic solar cells with the highest efficiency of 9.5%, *Adv. Energy Mater.* 8 (13) (2018), 1701942.
- [24] H. Wu, C. Zhang, K. Ding, L. Wang, Y. Gao, J. Yang, Efficient planar heterojunction perovskite solar cells fabricated by in-situ thermal-annealing doctor blading in ambient condition, *Org. Electron.* 45 (2017) 302–307.
- [25] S. Dong, K. Zhang, B. Xie, J. Xiao, H.-L. Yip, H. Yan, F. Huang, Y. Cao, High-performance large-area organic solar cells enabled by sequential bilayer processing via nonhalogenated solvents, *Adv. Energy Mater.* 9 (1) (2019), 1802832.
- [26] G. Ji, W. Zhao, J. Wei, L. Yan, Y. Han, Q. Luo, S. Yang, J. Hou, C.Q. Ma, 12.88% efficiency in doctor-blade coated organic solar cells through optimizing the surface morphology of a ZnO cathode buffer layer, *J. Mater. Chem. A* 7 (1) (2019) 212–220.
- [27] Y. Lin, L. Yu, Y. Xia, Y. Firdaus, S. Dong, C. Müller, O. Inganäs, F. Huang, T. D. Anthopoulos, F. Zhang, L. Hou, One-step blade-coated highly efficient nonfullerene organic solar cells with a self-assembled interfacial layer enabled by solvent vapor annealing, *Sol. RRL* 3 (8) (2019), 1900179.
- [28] C.Y. Jiang, V. Chellappan, W.P. Goh, J. Zhang, Investigating coating method induced vertical phase distribution in polymer-fullerene organic solar cells, *Sol. Energy Mater. Sol. Cells* 179 (2018) 241–246.
- [29] J. Xiong, J. Yang, B. Yang, C. Zhou, X. Hu, H. Xie, H. Huang, Y. Gao, Efficient and stable inverted polymer solar cells using TiO₂ nanoparticles and analyzed by Mott-Schottky capacitance, *Org. Electron.* 15 (8) (2014) 1745–1752.
- [30] S.K. Hau, H.-L. Yip, N.S. Baek, J. Zou, K. O'Malley, A.K.-Y. Jen, Air-stable inverted flexible polymer solar cells using zinc oxide nanoparticles as an electron selective layer, *Appl. Phys. Lett.* 92 (25) (2008), 253301.
- [31] J. Xiong, B. Yang, C. Zhou, J. Yang, H. Duan, W. Huang, X. Zhang, X. Xia, L. Zhang, H. Huang, Y. Gao, Enhanced efficiency and stability of polymer solar cells with TiO₂ nanoparticles buffer layer, *Org. Electron.* 15 (4) (2014) 835–843.
- [32] F.J. Lim, K. Ananthanarayanan, J. Luther, G.W. Ho, Influence of a novel fluorosurfactant modified PEDOT:PSS hole transport layer on the performance of inverted organic solar cells, *J. Mater. Chem.* 22 (48) (2012) 25057–25064.
- [33] M.Y. Ameen, P. Shamjid, T. Abhijith, T. Radhakrishnan, V.S. Reddy, Stability enhancement of P3HT:PCBM polymer solar cells using thermally evaporated MoO₃ anode buffer layer, *Phys. B: Phys. Condens. Matter* 530 (1) (2018) 201–207.
- [34] K. Zilberberg, S. Trost, J. Meyer, A. Kahn, A. Behrendt, D. Lützenkirchen-Hecht, R. Frahm, T. Riedl, Inverted organic solar cells with sol-gel processed high work-function vanadium oxide hole-extraction layers, *Adv. Funct. Mater.* 21 (24) (2011) 4776–4783.
- [35] Y. Wang, B. He, H. Wang, J. Xu, T. Ta, W. Li, Q. Wang, S. Yang, Y. Tang, B. Zou, Transparent WO₃/Ag/WO₃ electrode for flexible organic solar cells, *Mater. Lett.* 188 (2017) 107–110.
- [36] C. Zhang, Q. Luo, H. Wu, H. Li, J. Lai, G. Ji, L. Yan, X. Wang, D. Zhang, J. Lin, L. Chen, J. Yang, C. Ma, Roll-to-roll micro-gravure printed large-area zinc oxide thin film as the electron transport layer for solution-processed polymer solar cells, *Org. Electron.* 45 (2017) 190–197.
- [37] K. Xiong, L. Hou, M. Wu, Y. Huo, W. Mo, Y. Yuan, S. Sun, W. Xu, E. Wang, From spin coating to doctor blading: a systematic study on the photovoltaic performance of an isoindigo-based polymer, *Sol. Energy Mater. Sol. Cells* 132 (2015) 252–259.
- [38] N. Espinosa, R. García-Valverde, A. Urbina, F.C. Krebs, A life cycle analysis of polymer solar cell modules prepared using roll-to-roll methods under ambient conditions, *Sol. Energy Mater. Sol. Cells* 95 (5) (2011) 1293–1302.
- [39] J.C. Wang, W.T. Weng, M.Y. Tsai, M.K. Lee, S.F. Horng, T.P. Perng, C.C. Kei, C. C. Yu, H.F. Meng, Highly efficient flexible inverted organic solar cells using atomic layer deposited ZnO as electron selective layer, *J. Mater. Chem.* 20 (5) (2010) 862–866.
- [40] Q. Xie, X. Zheng, D. Wu, X. Chen, J. Shi, X. Han, X. Zhang, G. Peng, Y. Gao, H. Huang, High electrical conductivity of individual epitaxially grown MoO₂ nanorods, *Appl. Phys. Lett.* 111 (9) (2017), 093505.
- [41] G. Zhang, R. Xia, Z. Chen, J. Xiao, X. Zhao, S. Liu, H.-L. Yip, Y. Cao, Overcoming space-charge effect for efficient thick-film non-fullerene organic solar cells, *Adv. Energy Mater.* 8 (25) (2018), 1801609.
- [42] Y. Zhang, D. Deng, Z. Wang, Y. Wang, J. Zhang, J. Fang, Y. Yang, G. Lu, W. Ma, Z. Wei, Enhancing the photovoltaic performance via vertical phase distribution optimization in small molecule:PC₇₁BM blends, *Adv. Energy Mater.* 7 (22) (2017), 1701548.
- [43] H.J. Snaith, L. Schmidt-Mende, M. Grätzel, M. Chies, Light intensity, temperature, and thickness dependence of the open-circuit voltage in solid-state dye-sensitized solar cells, *Phys. Rev. B* 74 (4) (2006), 045306.
- [44] B. Yang, S. Zhang, S. Li, H. Yao, W. Li, J. Hou, A Self-organized poly (vinylpyrrolidone)-based cathode interlayer in inverted fullerene-free organic solar cells, *Adv. Mater.* 31 (2) (2018), e1804657.
- [45] U.K. Aryal, N. Chakravarthi, H.-Y. Park, H. Bae, S.-H. Jin, Y.S. Gal, Highly efficient polyacetylene-based polyelectrolytes as cathode interfacial layers for organic solar cell applications, *Org. Electron.* 53 (2018) 265–272.
- [46] N. Li, B.E. Lassiter, R.R. Lunt, G. Wei, S.R. Forrest, Open circuit voltage enhancement due to reduced dark current in small molecule photovoltaic cells, *Appl. Phys. Lett.* 94 (2) (2009), 023307.
- [47] X. Liu, L. Ye, W. Zhao, S. Zhang, S. Li, G.M. Su, C. Wang, H. Ade, J. Hou, Morphology control enables thickness-insensitive efficient nonfullerene polymer solar cells, *Mater. Chem. Front.* 1 (10) (2017) 2057–2064.
- [48] Z. Zhang, Z. Zhang, B. Zhao, Y. Huang, J. Xiong, P. Cai, X. Xue, J. Zhang, S. Tan, Polymer with 3D conductive network: thickness-insensitive electron transport layer for inverted polymer solar cells, *J. Mater. Chem. A* 6 (27) (2018) 12969–12973.
- [49] W. Yu, L. Huang, D. Yang, P. Fu, L. Zhou, J. Zhang, C. Li, Efficiency exceeding 10% for inverted polymer solar cells with ZnO/ionic liquid combined cathode interfacial layer, *J. Mater. Chem. A* 3 (20) (2015) 10660–10665.
- [50] Y. Wang, Q. Luo, N. Wu, Q. Wang, H. Zhu, L. Chen, Y.-Q. Li, L. Luo, C.Q. Ma, Solution-processed MoO₃:PEDOT:PSS hybrid hole transporting layer for inverted polymer solar cells, *ACS Appl. Mater. Interfaces* 7 (13) (2015) 7170–7179.